






Cite this: *Nanoscale*, 2023, **15**, 5083

Growth of 1D ClAlPc molecular chains mediated by graphene moiré patterns†

Haojie Guo,  *^a Mariano D. Jiménez-Sánchez,  ^a
Antonio J. Martínez-Galera  *^{b,c} and José M. Gómez-Rodríguez  ‡^{a,b,d}

The on-surface formation of iso-oriented 1D molecular architectures, with high structural perfection, on 2D materials has been a long-sought objective. However, such realization has been troublesome and limited, and it still remains an experimental challenge. Here, the quasi-1D stripe-like moiré pattern, arising at the interface of graphene grown on Rh(110), has been used to guide the formation of 1D molecular wires of π -conjugated, non-planar, chloro-aluminum phthalocyanine (ClAlPc) molecules, brought together by van der Waals interactions. Using scanning tunnelling microscopy (STM) under ultra-high vacuum (UHV) at 40 K, the preferential adsorption orientations of the molecules at low coverages have been investigated. The results shed light on the potential signature of graphene lattice symmetry breaking, induced by the incommensurate quasi-1D moiré pattern of Gr/Rh(110), as the subtle mechanism behind this templated growth of 1D molecular structures. For coverages close to 1 ML, the molecule–molecule interactions favor a closely packed square lattice arrangement. The present work provides new insights to tailor 1D molecular structures on graphene grown on a non-hexagonal metal substrate.

Received 7th November 2022,
Accepted 3rd February 2023

DOI: 10.1039/d2nr06237b

rsc.li/nanoscale

Introduction

The increasingly growing development of supramolecular chemistry has boosted the research on one-dimensional (1D) organic architectures over the last few years. This has allowed the observation of one-dimensional systems, developed from molecular units as building blocks, with very exciting properties such as Yu-Shiba-Rusinov bound states,¹ topological phases,² or enhanced single-molecule superradiance.³ From the application point of view, important achievements, such as the observation of high conductivity in doped polyacetylene,⁴ charge distribution control,⁵ and the development of prototypes of molecule-based logic gates,^{6,7} among others, have been accomplished in 1D organic systems. Tailoring such low

dimensional architectures was possible by engineering STM tip-assisted manipulation of individual molecules, edge-templated assembly, or diverse on-surface synthesis strategies that rely on predefined chemical precursor species.^{1–3,5–9}

The growth of 1D supramolecular structures driven mainly by dispersive intermolecular forces is much more challenging than when it is predominantly governed by other non-covalent interactions such as hydrogen bonding or metal–ligand bonding, which are stronger and more directional. In general, the formation of on-surface molecular architectures *via* dispersive interactions is ruled by a subtle interplay between molecule–molecule and molecule–substrate interactions, in which the local polarizability of the supporting surface plays a major role.¹⁰

Moiré patterns formed at the interfaces between a one-atom thick graphene sheet and a metal surface are often found to exhibit a chemical modulation, which is transformed into a specific charge distribution following the geometry of these superstructures.^{10–13} On the other hand, it is known that the symmetry of the underlying metal surface can be used to define the geometry of the moiré superperiodicities.¹⁴ In particular, while surfaces characterized by atomic arrangements with hexagonal symmetry result in moiré patterns with hexagonal symmetry,^{15–18} fringe-like quasi-1D moiré patterns are often obtained when the underlying support has a square or rectangular geometry.^{19–23} By taking advantage of this fact, these graphene–metal surfaces can be used to guide the molecular assembly in specific directions.

^aDepartamento de Física de la Materia Condensada, Universidad Autónoma de Madrid, E-28049 Madrid, Spain. E-mail: haojie.guo@uam.es

^bDepartamento de Física de Materiales, Universidad Autónoma de Madrid, E-28049 Madrid, Spain. E-mail: antonio.galera@uam.es

^cInstituto Nicolás Cabrera, Universidad Autónoma de Madrid, E-28049 Madrid, Spain

^dCondensed Matter Physics Center (IFIMAC), Universidad Autónoma de Madrid, E-28049 Madrid, Spain

† Electronic supplementary information (ESI) available: ClAlPc and CuPc molecules measured at RT; the square lattice structure of ClAlPc for coverages close to 1 ML; the molecular transition from 1D to 2D networks; molecular disorder on rotated domains of graphene grown on Rh(110). See DOI: <https://doi.org/10.1039/d2nr06237b>

‡ Deceased.



The moiré patterns of graphene–metal systems have been used to create different well-defined and long-range ordered 2D molecular structures.^{24–28} However, the formation of 1D molecular arrangements on graphene has been limited and scarce. A few examples are reported in the literature, based on the surface coordination reaction between molecules and metal adatoms^{8,9} and on the site-selective adsorption of magnetic phthalocyanines within the highly corrugated moiré patterns formed in graphene grown on Co, Fe intercalated Gr/Ir(111)²⁶ or Gr/Ru(0001).²⁹ Nevertheless, to date, the direct use of fringe-like moiré patterns to guide the growth of 1D molecular architectures has remained unsuccessful.

This work presents the moiré pattern-guided growth of equally oriented 1D molecular wires composed of individual polar chloro-aluminium phthalocyanine (ClAlPc) molecules, brought together by van der Waals interactions, on Gr/Rh(110) surfaces, which are characterized by the coexistence of rotational domains with quasi-1D moiré patterns.³⁰ As revealed by STM imaging at 40 K, the moiré pattern arising from the alignment, or near alignment, of the atomic lattice of graphene in the Rh[001] direction plays a crucial role as a guide for the formation of molecular chains at low molecular coverages. For high molecular coverages, the growth of 1D molecular arrays of ClAlPc becomes unfavourable, and a phase transition towards a more densely packed square lattice configuration takes place. This behaviour is explained as the result of the delicate interplay between dispersive attractive intermolecular interactions and repulsive ones, arising from the permanent dipole moment of ClAlPc, in combination with an effect of the moiré pattern, which is rationalized in terms of the symmetry breaking of the graphene lattice due to the quasi-1D moiré pattern modulation.

Experimental

Experiments were performed in an UHV system (a base pressure below 10^{-10} Torr) composed of two chambers. One chamber is equipped with standard sample cleaning facilities and evaporators for atomic or molecular deposition, and the other one hosts a home-built variable-temperature scanning tunnelling microscope (VT-STM). Both the chambers are interconnected by a gate valve, allowing the sample transfer without changing the UHV conditions. Graphene monolayers grown on Rh(110) were achieved through the thermal decomposition of ethylene (C_2H_4) on a hot metal substrate. In short, single-crystal Rh(110) was cleaned by cycles of Ar^+ sputtering at an incident energy of 1 keV, followed by annealing at 950 °C at an oxygen partial pressure of 2×10^{-6} Torr and flash annealing under UHV. The pristine Rh(110) surface was then exposed to an ethylene partial pressure of 3×10^{-7} Torr for 150 s, while simultaneously maintaining the metal substrate at 900 °C.

ClAlPc molecules were deposited on Gr/Rh(110) from a custom-built effusion cell while keeping the sample at RT. The evaporation rate was calibrated employing a quartz microbalance and further checked by STM imaging, yielding a deposition rate of ~ 0.25 ML min^{-1} . Here, 1 ML ($=4.5 \times 10^{13}$ mole-

cules cm^{-2}) refers to the saturation coverage of the molecular arrangement into a square lattice with 1.5 nm periodicity in the monolayer regime (after thermal treatment). Since the grown molecules form a bilayer structure regardless of the deposited amount, the sample was annealed at 300 °C for 15 minutes to obtain monolayers. A similar procedure has been applied for the deposition of CuPc on Gr/Rh(110), except for the annealing step since the CuPc already forms monolayers at RT.

All STM measurements were carried out with the sample cooled down at 40 K, to avoid molecular diffusion. The high mobility of the molecules is inferred based on the impossibility of STM to image the molecules at RT. This can be observed clearly in Fig. S1 (see the ESI†), where the recorded STM images are generally blurred. However, when the samples are cooled down to 40 K, all the molecules can be easily observed in STM.

The STM images were recorded in a constant current mode, using electrochemically etched tungsten tips, and with the bias voltage applied to the sample. The acquired data and their post-analysis were executed using the WSxM software.³¹

Results and discussion

As a reference, the chemical structure of the ClAlPc molecule is shown in Fig. 1. This molecule is non-planar due to the aluminium–chlorine bond unit in the center, lying orthogonal to the molecular plane. Because of the different electronegativity between aluminium and chlorine atoms, this phthalocyanine molecule has a permanent dipole moment perpendicular to its molecular plane.³² When it is adsorbed on a surface, the molecule can preferentially adopt two possible layouts, depending on whether the ending chlorine atom points toward the vacuum (Cl-up configuration) or toward the substrate (Cl-down).

Fig. 2 summarizes the sample morphology and the structural properties of ClAlPc deposited on Gr/Rh(110) surfaces, as well as the effects of a post-growth mild temperature anneal-

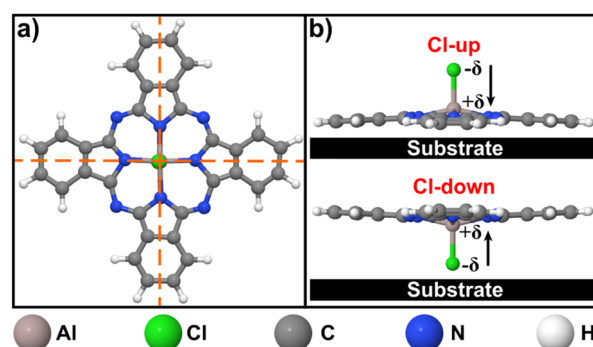


Fig. 1 Molecular structure of ClAlPc. (a) Top view of ClAlPc. The dashed orange lines indicate the molecular high symmetry axes. (b) Side views of Cl-up and Cl-down adsorption configurations, referring to the substrate, of ClAlPc molecules.



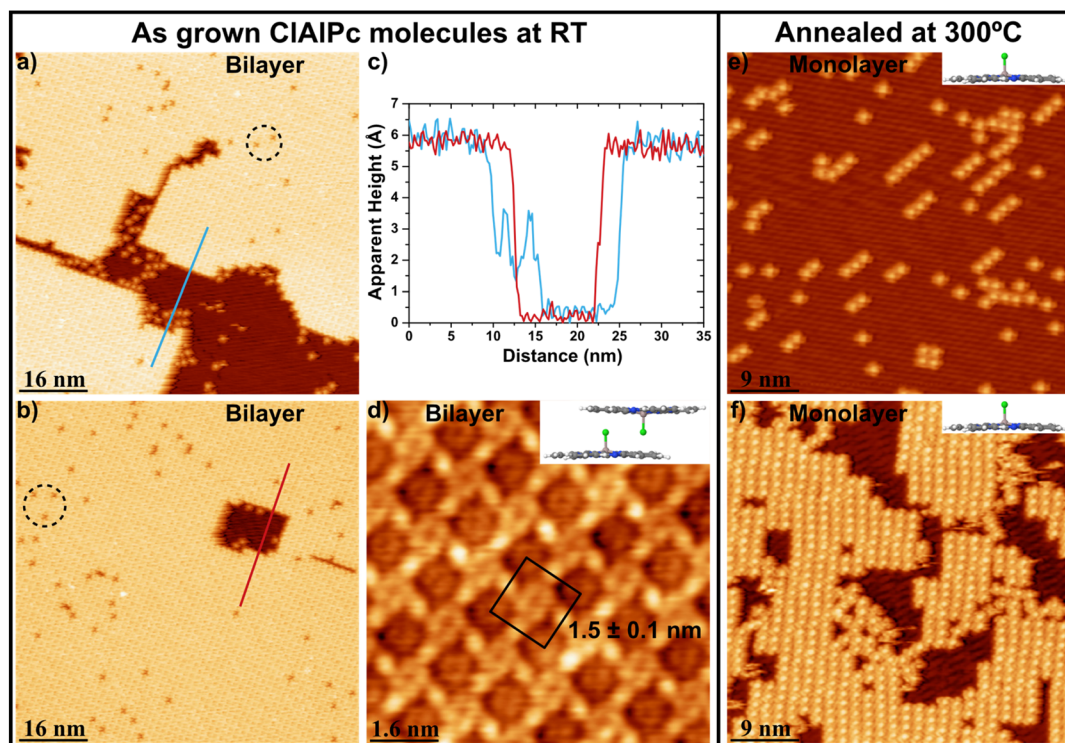


Fig. 2 Sample morphology and structural properties of CIAIPc on Gr/Rh(110), as well as the effect of thermal annealing characterized at 40 K. (a and b) Large-scale STM images after depositing two different amounts of CIAIPc molecules on Gr/Rh(110) at RT, without further annealing. The black circles indicate molecular vacancies. (c) Apparent height profiles across the coloured lines drawn in (a) and (b). (d) Close-up STM image of the bilayer structure of CIAIPc. The CIAIPc molecules adopt a Cl-down configuration in the 2nd layer and Cl-up layout in the 1st layer. (e and f) STM images after the same samples shown in (a) and (b), respectively, were annealed at 300 °C for 15 minutes. Depending on the initial coverage, the molecules now form a chain-like or square structure, adopting in both cases a Cl-up configuration. Tunnelling parameters: (a) $V_s = 2.0$ V; $I_t = 20$ pA; 80×80 nm². (b) $V_s = 2.0$ V; $I_t = 20$ pA; 80×80 nm². (d) $V_s = 2.2$ V; $I_t = 35$ pA; 8×8 nm². (e) $V_s = 1.8$ V; $I_t = 20$ pA; 45×45 nm². (f) $V_s = 2.0$ V; $I_t = 20$ pA; 45×45 nm².

ing. Fig. 2a and b show two large-scale STM images acquired after depositing, respectively, ~ 0.2 ML and ~ 1 ML of CIAIPc on a freshly grown Gr/Rh(110) substrate. In both cases, the molecules were deposited onto the target surface by keeping the latter at RT, and no further annealing was performed. In each case, closely packed islands are found to coexist with individual molecules, displaying a central protrusion. The measured apparent height of these islands is ~ 6 Å, as can be deduced from the profiles depicted in Fig. 2c obtained along the coloured lines indicated in Fig. 2a and b. A close-up STM image of one of those closely packed islands grown at RT, without post-growth annealing, is shown in Fig. 2d. A square superstructure with a lattice constant of 1.5 ± 0.1 nm can be observed in the image.

Fig. 2e and f show the corresponding STM images of the samples analysed in Fig. 2a and b after a subsequent mild temperature annealing at 300 °C for 15 minutes. As can be noted, in the post-growth annealed samples, all the CIAIPc molecules now show a protruding feature in their center. Interestingly, the molecular arrangement strongly depends on coverage. Specifically, at low coverages, CIAIPc seems to form chain-like structures, whereas, at high coverages, a square lattice rules the molecular disposition.

On the basis of the four-fold symmetry characteristic of phthalocyanine molecules³³ (see also Fig. 1a), the presence of features, as marked by the dashed black circles in Fig. 2a and b, imaged as a cross depression within the islands, can be associated with single-molecule vacancies. Concerning the molecular arrangement within these islands, Fig. 2c suggests that they correspond to a bilayer structure of CIAIPc since their apparent height is roughly twice that of the molecules with a central protruding dot. Moreover, in light of the general assignment in the literature,^{34–37} it is reasonable to assume that the CIAIPc molecule with a Cl-up configuration should have a central protrusion when observed in STM images, while in the Cl-down layout the molecules should be relatively flat, as the case of molecules in the islands. Therefore, CIAIPc molecules deposited at RT on Gr/Rh(110) mostly form bilayer structures regardless of the deposited amount, which are expected to consist of a staggered Cl-up and Cl-down arrangement for the first and second layer, respectively (see the schematic representation of the inset in Fig. 2d). Such stacking configuration has been proposed to minimize the electrostatic repulsion between CIAIPc molecules of the same layer, whose dipole moments are equally oriented.³⁸ On the other hand, extended regions of the CIAIPc monolayer have never been



found in the experiments when molecules are deposited on the substrate held at RT. A similar sample morphology was also reported for ClAlPc grown on graphene,^{39,40} graphite,^{35,38,39,41} and h-BN⁴² at RT. However, it differs from that of noble metals,^{43–47} in which the interaction with ClAlPc is expected to be stronger, where molecules always form monolayers, adopting a mixture of Cl-up and Cl-down configurations at the same time.

A different scenario is found when the samples in Fig. 2a and b were annealed at 300 °C for 15 minutes. In both cases, all the molecules now exhibit a protrusion in their center, indicating that they adopt a Cl-up configuration (see Fig. 2e and f). No bilayer structures of ClAlPc molecules were found throughout the entire sample. This effect could be due to thermal-induced desorption of the molecules in the 2nd layer, which would explain the much smaller molecular density found over the Gr/Rh(110) surfaces after annealing, although thermal-activated diffusion and reorientation processes of molecules of the 2nd layer into the 1st layer could also occur. Analogous bilayer-monolayer transition of the ClAlPc molecules caused by mild temperature annealing was observed for ClAlPc on graphite,³⁸ graphene⁴⁰ and h-BN.⁴² On Au(111)⁴³ and Ag(111),⁴⁶ thermal annealing only triggers a change in the molecular orientation, forcing all the ClAlPc molecules to adopt a Cl-up configuration.

Once the arrangement of the ClAlPc molecules deposited at RT and the post-growth annealing effects are established, the submonolayer regime of one-molecule thick structures of ClAlPc on Gr/Rh(110) was further investigated. This means that, from now on, all the samples were subjected to the post-growth annealing process. Fig. 3a shows a representative large-scale STM image of the samples with low molecular coverages (typically below 0.20 ML), displaying some individual molecules and clusters together with molecular wires of different lengths. Interestingly, the 1D molecular structures are oriented in the same direction. Fig. 3b depicts a zoom-in STM image within the region indicated by the dashed blue square in Fig. 3a. Apart from the molecular 1D architectures, this image reveals a stripe-like modulation on the Gr/Rh(110) surface, indicated by the green line, whose direction is parallel to the chain's network. Moreover, the lateral distance between the adjacent molecules in the wires is measured to be 1.4 ± 0.1 nm and all the molecules show a central protruding feature, which, as already discussed, is a clear sign that they adopt a Cl-up configuration. Fig. 3c–e show the representative STM images of the samples with increasing ClAlPc coverages on the Gr/Rh(110) surface. As observed, in the low coverage regime (<0.2 ML), the molecular wires predominate across the entire surface. Upon increasing the total amount of molecules, the 1D molecular architectures are transformed into a 2D arrangement exhibiting a closely packed square structure (see also Fig. S2 in the ESI†). For coverages between 0.08 ML and 0.17 ML, the histogram compiling the lengths of different ClAlPc nanowires is depicted in Fig. 3f, indicating that 1D nanostructures integrated by as large as 11 molecules were attained. In both cases, the sampling range was 930 nanowires, analysed

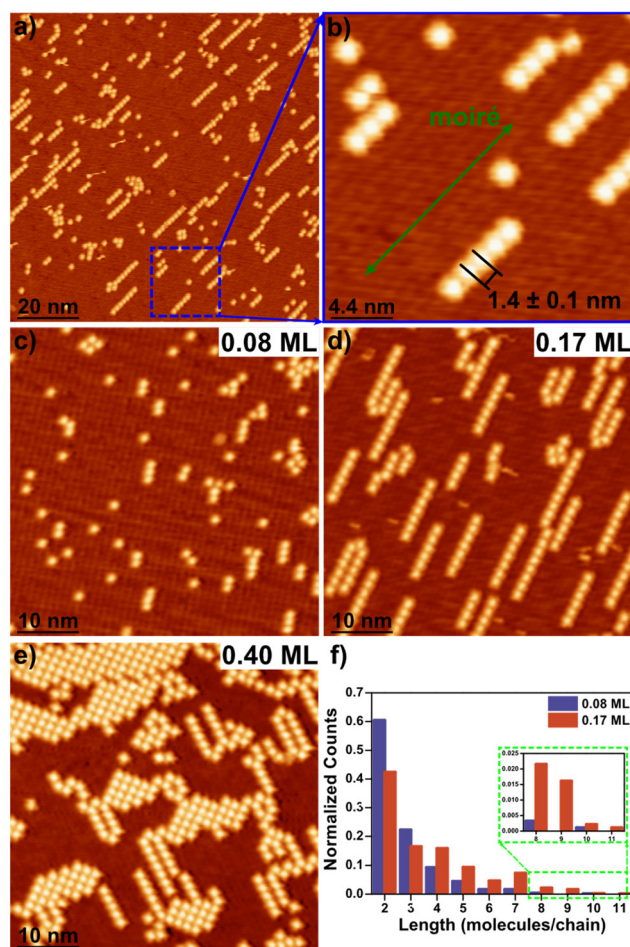


Fig. 3 1D molecular structure of ClAlPc measured at 40 K. (a) Large-scale STM image showing different molecular chain lengths of ClAlPc on Gr/Rh(110). (b) Zoom-in STM image, within the region marked by the dashed blue square in (a), where the substrate moiré pattern is resolved along with the chains. (c–e) Representative STM images illustrating the evolution of the ClAlPc chain structure for different coverages. (f) Histogram of the ClAlPc chain length for molecular coverages of 0.08 ML and 0.17 ML. The inset shows a magnified view for length ≥ 8 molecules per chain. Tunnelling parameters: (a) $V_s = 2.0$ V; $I_t = 40$ pA; 100×100 nm². (b) $V_s = 2.0$ V; $I_t = 40$ pA; 22×22 nm². (c) $V_s = 2.2$ V; $I_t = 20$ pA; 50×50 nm². (d) $V_s = 2.2$ V; $I_t = 20$ pA; 50×50 nm². (e) $V_s = 2.0$ V; $I_t = 20$ pA; 50×50 nm².

from the STM images acquired on several different regions of various samples.

As previously reported,³⁰ graphene monolayers grown on Rh(110) can adopt angular orientations within the intervals of $(-10^\circ, 0^\circ)$ and $(0^\circ, 10^\circ)$ as measured between the 2D material lattice and the [001] direction of the underlying metal, with a preference for angles around 0° and $\pm 10^\circ$. Precisely, for twist angles around 0° (aligned), the surface presents incommensurate quasi-1D moiré patterns, which are parallel, or nearly parallel, to the graphene lattice, with a separation of ~ 1 nm between moiré fringes. For other possible rotational angles, the resulting moiré patterns of Gr/Rh(110) are rather complex, featuring two sets of moiré fringes, with the respective periodicities of ~ 1 nm and ~ 4 –6 nm.



Taking the above description into consideration, it results logically to ascribe the stripe-like modulation, observed in Fig. 3b, with a moiré pattern of the Gr/Rh(110) surface. Concretely, it should correspond to the case in which the lattice of graphene is aligned, or nearly aligned, to the Rh[001] crystallographic direction, in light of the absence of the second set of moiré stripes on the surface. Hence, the ClAlPc molecular nanowires are oriented in the same direction as the underlying moiré stripes. It suggests a possible influence of the moiré structure on the formation of the 1D nanostructures, which will be discussed later.

From Fig. 3c, d and f, it is drawn that the length of the molecular nanowires can be tuned by increasing the number of predeposited molecules on the surface. Nevertheless, such a tuning window is very narrow since, as observed in Fig. 3f, there is a preference for the formation of short-length wires: nanowires with a number of molecules larger than 8 only constitute a reduced fraction of the total number, which may suggest that the interplay between molecule–molecule and molecule–substrate interactions does not favour the long-range growth of this chain-like structure. Also, it is interesting to point out that upon reaching a specific threshold coverage, the square lattice structure starts to dominate the molecular arrangement (see Fig. 3e) and ultimately collapses the entire surface for coverages close to 1 ML (see Fig. S2 in the ESI†). This means that the chain-like structure of ClAlPc constitutes a low coverage phase. Such an idea is further strengthened because the molecular wires are aligned with the diagonal of the square lattice structure (see Fig. S3 in the ESI†). Hence, the square lattice could be obtained *via* the formation of two chains next to each other, with a relative shift between them of half a molecule along the wires.

It is noteworthy to dedicate a few words to the formation temperature and the thermal stability of these 1D molecular chains. As has been stated in the Experimental section, it is impossible to image the ClAlPc molecules at RT (see Fig. S1 in the ESI†), neither individual molecules nor ordered structures. This fact has been rationalized in terms of an elevated diffusion rate of the molecules at RT, being responsible for a high mobility. Therefore, this led to the conclusion that the 1D molecular chains should be unstable at RT, and consequently at higher temperatures. However, when the samples were cooled down to 40 K, the 1D molecular chains do emerge on the surface as can be observed, for instance, in Fig. 3. Hence, the formation of this 1D structure should occur in the temperature range between RT and 40 K, with stability guaranteed at least at 40 K.

To gain a deeper insight into the effect of the moiré pattern of Gr/Rh(110) on the formation of the molecular wires, the orientation of the high symmetry axes of the ClAlPc molecule with respect to the moiré pattern was investigated. Fig. 4a–e show STM images where the molecular axes of ClAlPc molecules are resolved along with the substrate moiré pattern. As indicated by the superimposed blue and red crosses, on the graphene/Rh(110) surfaces, the molecular axes of ClAlPc are rotated by either 45° (type A) or 75° (type B) with respect to the moiré direction. In the case of dimers (see Fig. 4b and c), the

1D nanostructures are formed either by two molecules of type A or by a mixture of type A and type B. When the number of molecules per chain is larger than 2 (see Fig. 4d and e), the nanowires are always formed by an alternating combination of type A and type B molecules.

To tackle these observations, schematic representations that could explain these two specific orientations of the ClAlPc molecules with respect to the moiré fringes are shown in Fig. 4f–h. For simplicity, it has been assumed in these representations that the molecules are placed on the aligned graphene domain. As stated earlier, the moiré patterns of aligned, or nearly aligned, domains are incommensurate, and the moiré pattern is parallel, or nearly parallel, to the atomic lattice of graphene and the Rh[001] direction. Under this framework, for a twist angle of around 15° between the molecular axis and a high symmetry direction of the graphene lattice, the resulting molecular axis orientations with respect to the moiré pattern reproduce the experimental observations depicted in Fig. 4a–e.

The assumption that the molecules are located on aligned, or nearly aligned, graphene with respect to the Rh[001] direction is founded on the presence of only one set of moiré stripes on those regions where the ClAlPc molecules form 1D nanostructures (see STM images in Fig. 3 and 4). In contrast, on the areas showing two sets of moiré stripes, the molecules are adsorbed randomly on the surface and do not form, in a uniform way, chain-like or closely packed square structures (see Fig. S4 in the ESI†). It should be noted that the presence of two sets of moiré fringes is characteristic of graphene rotated with respect to Rh(110).

Nanowire formation along the moiré stripes of aligned, or nearly aligned, domains must be the result of an intricate balance between molecule–molecule and molecule–substrate interactions. The rotation angle of 15° between each of the two ClAlPc high symmetry axes and the graphene lattice, indicated in Fig. 4f–h, was also reported for ClAlPc grown on the Gr/Pt(111)⁴⁸ surface, which is characterized by the coexistence of multiple moiré patterns with hexagonal geometry. Thus, it seems that this adsorption configuration is the most stable for ClAlPc on the graphene lattice regardless the orientation and geometry of the moiré pattern. Nonetheless, nanowires grow along the moiré stripes. Then, the effect of the moiré pattern on the formation of these nanostructures of ClAlPc molecules could be understood in terms of the symmetry reduction of the graphene lattice, due to the incommensurate quasi-1D moiré patterns formed at the Gr/Rh(110) interface. This symmetry reduction could induce changes in the surface charge distribution, resulting in variations of the local polarizability across the moiré stripes, which would make favourable the molecular self-assembly along them. Definitively, the quasi-1D moiré pattern creates an anisotropy, which seems to favour the packing of ClAlPc molecules along the moiré stripes. It explains why molecular wires of ClAlPc are not found to be orientated along the other graphene lattice directions, which is the case of the much shorter CuPc, CoPc, and SnPc chains formed on graphite.^{49,50}



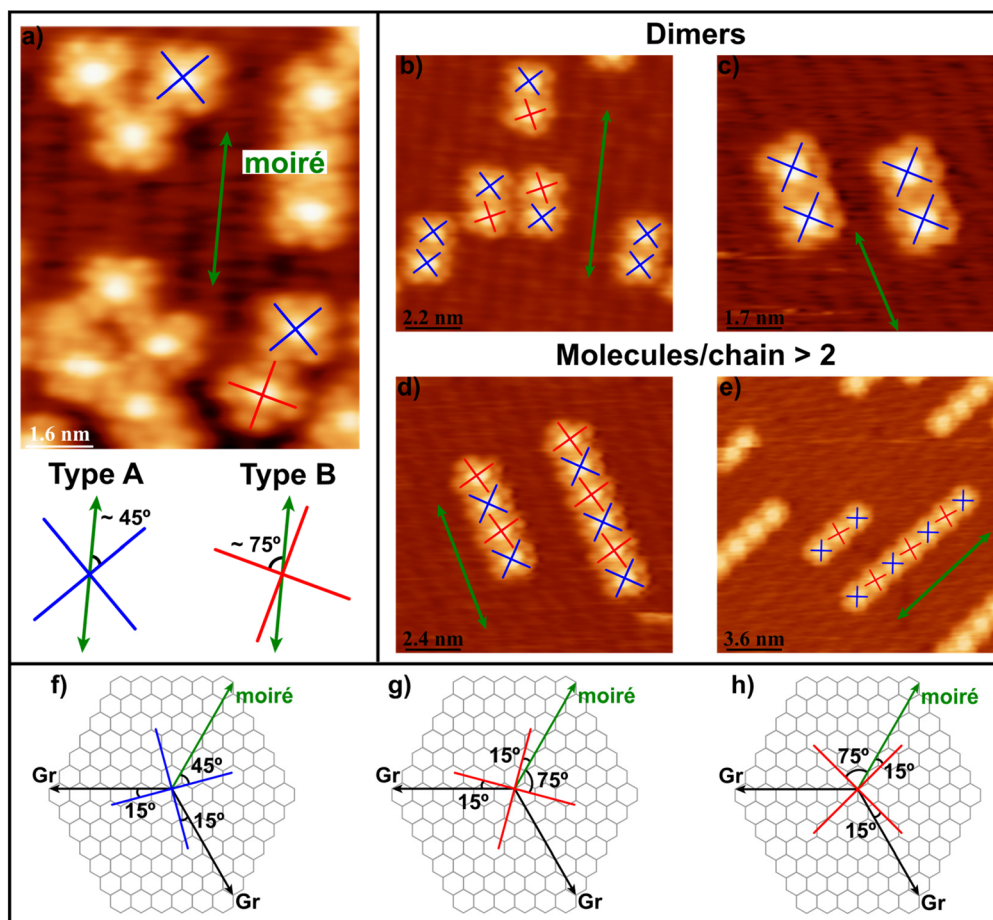


Fig. 4 Molecular orientation of CIAIPc chains measured at 40 K. (a) Orientation of the axis of CIAIPc molecules with respect to the substrate moiré pattern. (b and c) STM images revealing the two possible orientational configurations of the molecules when they form dimers: 45° – 45° or 45° – 75° . (d and e) STM images showing the mixed orientation of 45° and 75° configurations of the molecules when the length (molecules per chain) is > 2 . (f–h) Proposed schematic representation for the observed orientation of the CIAIPc molecules on Gr/Rh(110), based on the preferential alignment of the molecular axis with the graphene lattice direction. Likewise, it has been assumed that the CIAIPc molecules are adsorbed on the aligned domain of graphene with respect to the Rh[001] direction (see the main text for further reasoning). Tunnelling parameters: (a) $V_s = -1.8$ V; $I_t = 30$ pA; 8×10 nm 2 . (b) $V_s = 1.65$ V; $I_t = 80$ pA; 11×11 nm 2 . (c) $V_s = 2.0$ V; $I_t = 70$ pA; 8.5×8.5 nm 2 . (d) $V_s = 2.0$ V; $I_t = 30$ pA; 12×12 nm 2 . (e) $V_s = 2.0$ V; $I_t = 60$ pA; 20×20 nm 2 .

On the other hand, from the side of the molecule–molecule interaction, it comprises a repulsive term due to the dipole–dipole interaction between adjacent molecules, due to the Cl–Al group, and the attractive one, which is the result of the dispersive interactions between the π conjugated phthalocyanine rings. Also, it should be taken into account that both the dipole moment and the phthalocyanine ring can affect the surface potential landscape of the Gr/Rh(110) surface, which, in turn, would influence the molecule–substrate interaction. To disentangle the effects associated with both contributions to the net molecule–molecule interaction, and to shed light on the influence of the possible interactions mediated by the phthalocyanine ring, the behaviour of CuPc, which does not have a permanent dipole moment perpendicular to the molecular plane, on the Gr/Rh(110) surface has been studied (see Fig. 5). The planar and non-polar characters of the molecule can be deduced from the side view in Fig. 5a. This molecule was deposited on the surface following similar procedures to

those for the CIAIPc (see the Experimental section), except that, in this case, annealing was unnecessary since it forms directly monolayers after deposition. As can be observed from Fig. 5, the formation of isolated wires comprising more than two molecular units is hardly observed in this case. Moreover, from the comparison between STM images as shown in Fig. 5 with the ones displayed in Fig. 3 and 4, it seems that the electrostatic dipole–dipole interaction between CIAIPc molecules prevents, at low coverages, the formation of neighbour chains along consecutive moiré stripes of the graphene/Rh(110) surface, which, otherwise, would result in an arrangement following the square lattice. In contrast, it seems that the attractive term of the molecule–molecule interaction, associated with dispersive interactions between the π conjugated phthalocyanine rings, dominates over the repulsive term along the moiré stripes, which could be induced by the above mentioned anisotropy of the graphene layer due to the moiré pattern. Nonetheless, for chains comprising more than eight



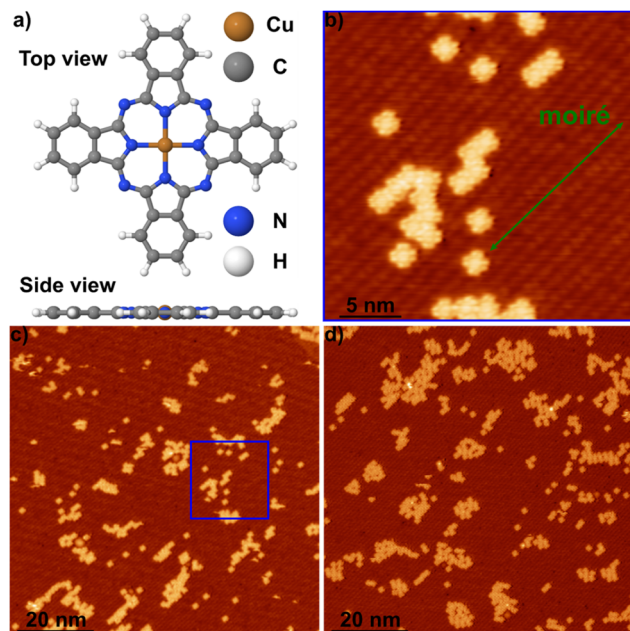


Fig. 5 CuPc on Gr/Rh(110) measured at 40 K. (a) Molecular structure of the planar and non-polar CuPc. (b) High resolution STM image of CuPc molecules on Gr/Rh(110) measured within the blue square indicated in (c) where the characteristic cross shape of Pc molecules is resolved. In contrast to ClAlPc molecules, the center of each CuPc molecule does not display a bright protrusion, which is consistent with the planar characteristic of CuPc. Additionally, short chains of CuPc molecules, aligned with the underlying moiré pattern, can be observed. (c and d) Representative STM images showing the overall sample morphology of CuPc molecules on Gr/Rh(110), where only a small portion of CuPc molecules forms 1D molecular chains. This may suggest that the formation of 1D molecular wires is less favoured for CuPc on the Gr/Rh(110) substrate. Therefore, the dipole moment of ClAlPc molecules could play a significant role in the structuring of the molecular chains of this molecule, as discussed in the main text. Tunnelling parameters: (b) $V_s = 1.5$ V; $I_t = 0.1$ nA; 25×25 nm². (c) $V_s = 1.8$ V; $I_t = 20$ pA; 100×100 nm². (d) $V_s = 1.8$ V; $I_t = 20$ pA; 100×100 nm².

units, the stress associated with the net repulsive interaction along the molecular structure seems to become dominant, given the fact that the fraction of wires exhibiting larger lengths is tiny (see Fig. 3f).

Conclusions

In summary, the formation of 1D molecular networks made of ClAlPc molecules on Gr/Rh(110) substrates has been investigated by STM under UHV at 40 K. The experimental results reveal that RT deposited molecules, without conducting further annealing, create bilayer structures of ClAlPc with an alternating Cl-up and Cl-down stacking configuration, like previous experiments on graphite and graphene. By performing mild annealing on these samples, the bilayer structure transforms into a monolayer with all the molecules assuming a Cl-up layout. Depending on the surface coverage, the deposited molecules in the monolayer adopt two possible molecular

arrangements. In the low coverage regime (<0.20 ML), the molecules form 1D molecular chains, in which the cohesive interaction between the molecular units within the chains is relatively weak and whose lengths can be tuned by the total amount of ClAlPc on the surface. As unveiled by STM, all the chains are oriented in the same direction as the underlying quasi-1D stripe-like moiré pattern of Gr/Rh(110). Moreover, high-resolution STM images of the molecular axis orientation with respect to the substrate suggest an influence of the moiré pattern on the positioning of ClAlPc on the surface, which, in turn, has a direct consequence on the formation of these molecular chains. In contrast, for coverages close to 1 ML, the ClAlPc molecules recover the well-known square lattice structure. The comparison of the behaviour of ClAlPc on Gr/Rh(110) with that of CuPc shows the respective roles played by the intermolecular interaction between permanent dipoles, the dispersive ones between the phthalocyanine rings, as well as the anisotropy associated with the moiré pattern, in the formation of the 1D molecular structures. It has allowed revealing the requisites that a certain molecular adsorbate must fulfill to give rise to equally oriented molecular wires on Gr/Rh(110) surfaces. That is, for the group of phthalocyanine molecules, the presence of a permanent dipole moment is a key factor in the formation of these 1D molecular nanostructures.

Conflicts of interest

There are no conflicts to declare.

Acknowledgements

The authors dedicate this work to the memory of Prof. José María Gómez Rodríguez, a personal friend, mentor and colleague. Financial support from the Spanish Ministerio de Economía y Competitividad (MINECO) and Fondo Europeo de Desarrollo Regional (FEDER) under grant no. MAT2016-77852-C2-2-R, as well as from the Spanish Ministerio de Ciencia e Innovación through the “María de Maetzu” program for units of excellence in R&D (grant no. CEX2018-000805-M) is gratefully acknowledged. A. J. M.-G. acknowledges funding by the Spanish MICINN through Project no. PID2020-116619GA-C22 and from the Comunidad de Madrid and the Universidad Autónoma de Madrid through project SI3/PJI/2021-00500.

References

- 1 S. Kezilebieke, M. Dvorak, T. Ojanen and P. Liljeroth, *Nano Lett.*, 2018, **18**, 2311–2315.
- 2 B. Cirera, A. Sanchez-Grande, B. de la Torre, J. Santos, S. Edalatmanesh, E. Rodriguez-Sanchez, K. Lauwaet, B. Mallada, R. Zboril, R. Miranda, O. Groning, P. Jelinek, N. Martin and D. Eciija, *Nat. Nanotechnol.*, 2020, **15**, 437–443.



- 3 Y. Zhang, Y. Luo, Y. Zhang, Y. J. Yu, Y. M. Kuang, L. Zhang, Q. S. Meng, Y. Luo, J. L. Yang, Z. C. Dong and J. G. Hou, *Nature*, 2016, **531**, 623–627.
- 4 C. K. Chiang, C. R. Fincher, Y. W. Park, A. J. Heeger, H. Shirakawa, E. J. Louis, S. C. Gau and A. G. Macdiarmid, *Phys. Rev. Lett.*, 1977, **39**, 1098–1101.
- 5 H.-Z. Tsai, J. Lischner, A. A. Omrani, F. Liou, A. S. Aikawa, C. Karrasch, S. Wickenburg, A. Riss, K. C. Natividad, J. Chen, W.-W. Choi, K. Watanabe, T. Taniguchi, C. Su, S. G. Louie, A. Zettl, J. Lu and M. F. Crommie, *Nat. Electron.*, 2020, **3**, 598–603.
- 6 A. J. Heinrich, C. P. Lutz, J. A. Gupta and D. M. Eigler, *Science*, 2002, **298**, 1381–1387.
- 7 M. Leisegang, A. Christ, S. Haldar, S. Heinze and M. Bode, *Nano Lett.*, 2021, **21**, 550–555.
- 8 F. Huttmann, N. Schleheck, N. Atodiresei and T. Michely, *J. Am. Chem. Soc.*, 2017, **139**, 9895–9900.
- 9 J. Li, L. Solianyk, N. Schmidt, B. Baker, S. Gottardi, J. C. M. Lopez, M. Enache, L. Monjas, R. van der Vlag, R. W. A. Havenith, A. K. H. Hirsch and M. Stohr, *J. Phys. Chem. C*, 2019, **123**, 12730–12735.
- 10 A. Kumar, K. Banerjee and P. Liljeroth, *Nanotechnology*, 2017, **28**, 082001.
- 11 J. Wintterlin and M. L. Bocquet, *Surf. Sci.*, 2009, **603**, 1841–1852.
- 12 C. Busse, P. Lazic, R. Djemour, J. Coraux, T. Gerber, N. Atodiresei, V. Caciuc, R. Brako, A. T. N'Diaye, S. Blugel, J. Zegenhagen and T. Michely, *Phys. Rev. Lett.*, 2011, **107**, 036101.
- 13 M. Batzill, *Surf. Sci. Rep.*, 2012, **67**, 83–115.
- 14 A. J. Martinez-Galera and J. M. Gomez-Rodriguez, *Nano Res.*, 2018, **11**, 4643–4653.
- 15 S. Marchini, S. Gunther and J. Wintterlin, *Phys. Rev. B: Condens. Matter Mater. Phys.*, 2007, **76**, 075429.
- 16 J. Coraux, A. T. N'Diaye, C. Busse and T. Michely, *Nano Lett.*, 2008, **8**, 565–570.
- 17 M. M. Ugeda, D. Fernandez-Torre, I. Brihuega, P. Pou, A. J. Martinez-Galera, R. Perez and J. M. Gomez-Rodriguez, *Phys. Rev. Lett.*, 2011, **107**, 116803.
- 18 A. Martin-Recio, C. Romero-Muniz, A. J. Martinez-Galera, P. Pou, R. Perez and J. M. Gomez-Rodriguez, *Nanoscale*, 2015, **7**, 11300–11309.
- 19 T. Gao, S. B. Xie, Y. B. Gao, M. X. Liu, Y. B. Chen, Y. F. Zhang and Z. F. Liu, *ACS Nano*, 2011, **5**, 9194–9201.
- 20 H. I. Rasool, E. B. Song, M. Mecklenburg, B. C. Regan, K. L. Wang, B. H. Weiller and J. K. Gimzewski, *J. Am. Chem. Soc.*, 2011, **133**, 12536–12543.
- 21 A. Locatelli, C. Wang, C. Africh, N. Stojic, T. O. Montes, G. Comelli and N. Binggeli, *ACS Nano*, 2013, **7**, 6955–6963.
- 22 O. Dugerjav, G. Duvjir, L. Tapaszto and C. Hwang, *J. Phys. Chem. C*, 2020, **124**, 12106–12111.
- 23 Z. Y. Zou, V. Carnevali, M. Jugovac, L. L. Patera, A. Sala, M. Panighel, C. Cepek, G. Soldano, M. M. Mariscal, M. Peressi, G. Comelli and C. Africh, *Carbon*, 2018, **130**, 441–447.
- 24 J. H. Mao, H. G. Zhang, Y. H. Jiang, Y. Pan, M. Gao, W. D. Xiao and H. J. Gao, *J. Am. Chem. Soc.*, 2009, **131**, 14136–14137.
- 25 J. Lu, P. S. E. Yeo, Y. Zheng, Z. Y. Yang, Q. L. Bao, C. K. Gan and K. P. Loh, *ACS Nano*, 2012, **6**, 944–950.
- 26 M. Bazarnik, J. Brede, R. Decker and R. Wiesendanger, *ACS Nano*, 2013, **7**, 11341–11349.
- 27 Q. Y. Zhou, Y. B. Li, Q. Li, Y. B. Wang, Y. L. Yang, Y. Fang and C. Wang, *Nanoscale*, 2014, **6**, 8387–8391.
- 28 K. Banerjee, A. Kumar, F. F. Canova, S. Kezilebieke, A. S. Foster and P. Liljeroth, *J. Phys. Chem. C*, 2016, **120**, 8772–8780.
- 29 K. Yang, W. D. Xiao, Y. H. Jiang, H. G. Zhang, L. W. Liu, J. H. Mao, H. T. Zhou, S. X. Du and H. J. Gao, *J. Phys. Chem. C*, 2012, **116**, 14052–14056.
- 30 A. J. Martinez-Galera, H. Guo, M. D. Jiménez-Sánchez, E. G. Michel and J. M. Gómez-Rodríguez, *Carbon*, 2023, **205**, 294–301.
- 31 I. Horcas, R. Fernandez, J. M. Gomez-Rodriguez, J. Colchero, J. Gomez-Herrero and A. M. Baro, *Rev. Sci. Instrum.*, 2007, **78**, 013705.
- 32 H. Fukagawa, S. Hosoumi, H. Yamane, S. Kera and N. Ueno, *Phys. Rev. B: Condens. Matter Mater. Phys.*, 2011, **83**, 085304.
- 33 J. M. Gottfried, *Surf. Sci. Rep.*, 2015, **70**, 259–379.
- 34 Y. L. Huang, Y. H. Lu, T. C. Niu, H. Huang, S. Kera, N. Ueno, A. T. S. Wee and W. Chen, *Small*, 2012, **8**, 1423–1428.
- 35 Y. L. Huang, R. Wang, T. C. Niu, S. Kera, N. Ueno, J. Pflaum, A. T. S. Wee and W. Chen, *Chem. Commun.*, 2010, **46**, 9040–9042.
- 36 S. Matencio, R. Palacios-Rivera, J. I. Martinez, C. Ocal and E. Barrena, *J. Phys. Chem. C*, 2018, **122**, 16033–16041.
- 37 T. C. Niu, N. Si, D. C. Zhou and M. Zhou, *J. Phys. Chem. C*, 2019, **123**, 7178–7184.
- 38 S. Kera, H. Yamane, H. Honda, H. Fukagawa, K. K. Okudaira and N. Ueno, *Surf. Sci.*, 2004, **566**, 571–578.
- 39 H. Y. Mao, R. Wang, Y. Wang, T. C. Niu, J. Q. Zhong, M. Y. Huang, D. C. Qi, K. P. Loh, A. T. S. Wee and W. Chen, *Appl. Phys. Lett.*, 2011, **99**, 093301.
- 40 Y. Ogawa, T. C. Niu, S. L. Wong, M. Tsuji, A. T. S. Wee, W. Chen and H. Ago, *J. Phys. Chem. C*, 2013, **117**, 21849–21855.
- 41 H. Y. Ma, Y. L. Zhao, M. W. Zaw, J. F. Jia, R. Q. Zhang and M. A. Van Hove, *Surf. Sci.*, 2019, **681**, 104–110.
- 42 H. J. Guo, M. Izquierdo-Cid, M. D. Jimenez-Sanchez, A. J. Martinez-Galera and J. M. Gomez-Rodriguez, *Adv. Mater. Interfaces*, 2021, **8**, 2101389.
- 43 Y. L. Huang, W. Chen, F. Bussolotti, T. C. Niu, A. T. S. Wee, N. Ueno and S. Kera, *Phys. Rev. B: Condens. Matter Mater. Phys.*, 2013, **87**, 085205.
- 44 T. C. Niu, M. Zhou, J. L. Zhang, Y. P. Feng and W. Chen, *J. Phys. Chem. C*, 2013, **117**, 1013–1019.
- 45 T. C. Niu, *Appl. Phys. Lett.*, 2015, **106**, 161601.
- 46 M. K. Lin, Y. Nakayama, Y. J. Zhuang, K. J. Su, C. Y. Wang, T. W. Pi, S. Metz, T. A. Papadopoulos, T. C. Chiang, H. Ishii



- and S. J. Tang, *Phys. Rev. B: Condens. Matter Mater. Phys.*, 2017, **95**, 085425.
- 47 H. J. Song, C. F. Fu, N. Li, H. Zhu, Z. T. Peng, W. H. Zhao, J. X. Dai, L. B. Xing, Z. C. Huang, W. Chen, Y. F. Wang, J. L. Yang and K. Wu, *Phys. Chem. Chem. Phys.*, 2017, **19**, 22401–22405.
- 48 M. D. Jimenez-Sanchez, N. Sanchez-Abad, N. Nicoara and J. M. Gomez-Rodriguez, *Surf. Sci.*, 2021, **710**, 121848.
- 49 K. Walzer and M. Hietschold, *Surf. Sci.*, 2001, **471**, 1–10.
- 50 M. Scheffler, L. Smykalla, D. Baumann, R. Schlegel, T. Hanke, M. Toader, B. Buchner, M. Hietschold and C. Hess, *Surf. Sci.*, 2013, **608**, 55–60.

